Biophysical Journal
Article

Biophysical Society

Binding Mechanism of the N-Terminal SH3 Domain of CrkII and Proline-Rich Motifs in cAbl

Veer S. Bhatt,[1] Danyun Zeng,[1] Inna Krieger,[1] James C. Sacchettini,[1] and Jae-Hyun Cho[1,*]
[1]Department of Biochemistry and Biophysics, Texas A&M University, College Station, Texas

ABSTRACT The N-terminal Src homology 3 (nSH3) domain of a signaling adaptor protein, CT-10 regulator of kinase II (CrkII), recognizes proline-rich motifs (PRMs) of binding partners, such as cAbl kinase. The interaction between CrkII and cAbl kinase is involved in the regulation of cell spreading, microbial pathogenesis, and cancer metastasis. Here, we report the detailed biophysical characterizations of the interactions between the nSH3 domain of CrkII and PRMs in cAbl. We identified that the nSH3 domain of CrkII binds to three PRMs in cAbl with virtually identical affinities. Structural studies, by using x-ray crystallography and NMR spectroscopy, revealed that the binding modes of all three nSH3:PRM complexes are highly similar to each other. Van 't Hoff analysis revealed that nSH3:PRM interaction is associated with favorable enthalpy and unfavorable entropy change. The combination of experimentally determined thermodynamic parameters, structure-based calculations, and ^{15}N NMR relaxation analysis highlights the energetic contribution of conformational entropy change upon the complex formation, and water molecules structured in the binding interface of the nSH3:PRM complex. Understanding the molecular basis of nSH3:PRM interaction will provide, to our knowledge, new insights for the rational design of small molecules targeting the interaction between CrkII and cAbl.

INTRODUCTION

The CT-10 regulator of kinase (Crk) oncogene was originally identified in avian retrovirus CT10 (1). Human Crk protein family consists of three isoforms, CrkI, CrkII, and CrkIII, and a homolog, CrkL (2–4). CrkII is a signaling adaptor protein that is involved in a variety of cellular processes, including proliferation, migration, invasion, and apoptosis, and its expression levels have been associated with aggressive lung, breast, and ovarian cancers (5–10). CrkII consists of three Src homology (SH) domains: SH2, the N-terminal SH3 (nSH3), and the C-terminal SH3 (cSH3) domains. As a signaling adaptor, CrkII mediates a number of protein-protein interactions, through its SH2 and SH3 domains (10,11). Among these three domains, the nSH3 plays a central role in the mediation of a number of protein-protein interactions, by recognizing proline-rich motifs (PRMs) (12–17).

Cellular nonreceptor tyrosine kinase cAbl is one of the major binding partners of CrkII (18–20). cAbl is a proto-oncoprotein, and it is involved in various cellular processes (21). The N-terminal half of cAbl consists of SH3, SH2, and kinase domain, while the C-terminal half of cAbl mainly consists of structurally disordered regions, which contain a variety of posttranslational modifications and linear motifs, such as phosphorylation, PRMs, and nuclear localization/export signals (21). PRMs in cAbl are essential for the modulation of filopodium formation during the attachment to the fibronectin-coated surfaces, through the interactions with SH3 domain-containing proteins, such as CrkII, Nck, and Grb2 (19,22,23). The interaction between CrkII and cAbl through PRMs results in the phosphorylation of CrkII (19), which leads to the inhibition of Crk signaling during attachment and an increased rate of filopodium formation. In contrast, the overexpression of Crk family proteins decreases filopodium formation, while enhancing lamellipodium formation (20,22).

The interactions between Crk family proteins and cAbl have bidirectional regulatory effects. For example, while the cAbl-mediated phosphorylation of CrkII regulates the function of CrkII, phosphorylated CrkII in turn transactivates cAbl kinase activity (24,25). In addition, the interaction between CrkII and cAbl is important for the development of anticancer drugs that are targeting the oncogenic form of cAbl, Bcr-Abl, which causes the development of chronic myeloid leukemia (18,26). Because of the importance of the interactions between CrkII and cAbl, they have been studied using various assays, such as yeast two-hybrid system, filter-binding assay, phage display screening, and pulldown

Submitted March 7, 2016, and accepted for publication May 4, 2016.
*Correspondence: jaehyuncho@tamu.edu
Veer S. Bhatt and Danyun Zeng contributed equally to this work.
Editor: David Eliezer.
http://dx.doi.org/10.1016/j.bpj.2016.05.008
© 2016 Biophysical Society.

assays (20,22). These studies revealed the presence of multiple PRMs in cAbl (PRM^{cAbl}), which mediate the interaction with the nSH3 domain of CrkII ($nSH3^{CrkII}$). However, the quantitative and detailed biophysical studies of the interactions between the nSH3 domain and individual PRMs in cAbl have not been conducted.

The thermodynamic principles underlying the interaction between SH3 domains and PRMs (SH3:PRM interactions) are not well understood. Despite the largely hydrophobic binding interface, SH3:PRM interaction is associated with a large favorable enthalpy and unfavorable entropic penalty (i.e., $\Delta H^{\circ}_{\text{bind}} < 0$ and $-T\Delta S^{\circ}_{\text{bind}} > 0$) (27–30). Various mechanisms have been proposed to explain the anomalous binding thermodynamics of SH3:PRM interaction. For example, the change in conformational dynamics of SH3 domains and PRMs has been considered a source of unfavorable binding entropy change (29). Additionally, the importance of water molecules at the binding interface of SH3:PRM complex in the binding thermodynamics has been demonstrated (27,31).

In this study, as a first step toward elucidating the interaction between CrkII and cAbl, we have carried out extensive studies of structures, thermodynamics, and conformational dynamics of $nSH3^{CrkII}$:PRM^{cAbl} interactions. We have investigated the binding of $nSH3^{CrkII}$ and all individual PRMs in the C-terminal disordered region of cAbl, and showed that the nSH3 domain binds to the three PRMs with similar affinity. To understand the binding mechanism of nSH3 and PRMs, we have determined the crystal structure of one of the three nSH3:PRM complexes. Moreover, the results of NMR chemical shift perturbation (CSP) study indicate that all three nSH3:PRM complexes have similar structures. The combination of the structure-based calculation of binding thermodynamics and NMR ^{15}N relaxation analysis allows understanding the molecular origin of binding free energy between nSH3 and PRM. These results also provide insights into the energetic contribution of water molecules at the binding interface and the conformational entropy of protein in protein-ligand interactions.

MATERIALS AND METHODS

Protein preparation

The protein samples used in this study were prepared using the *Escherichia coli* BL21 (DE3) expression system with a plasmid containing a gene for the nSH3 domain (residues 124–207) of human CrkII. The expression was induced with 0.5 mM IPTG (isopropyl β-D-1-thiogalactopyranoside) containing $^{15}NH_4Cl$. For the NMR triple-resonance assignment experiments, $^{13}C_6$ glucose was added to M9 medium, in addition to $^{15}NH_4Cl$. The expressed protein was purified using Ni-sepharose (HisTrap HP column; GE Healthcare Life Sciences, Marlborough, MA) and digested with TEV-protease to remove N-terminal His-tag. The nSH3 domain was further purified on a second Ni-sepharose column and an anion exchange column (Mono-Q; GE Healthcare Life Sciences). Protein concentration was determined by measuring UV absorbance at 280 nm.

Peptide ligands

Synthetic PRMs used in this study were purchased from LifeTein (Somerset, NJ) in a crude form, and further purified using reverse-phase high performance liquid chromatography in our laboratory. The N- and C-termini of peptides were acetylated and amidated, respectively. The peptide concentration was determined by measuring the UV absorption of a single tyrosine at the N- or C-terminal ends of the peptide.

Binding assay

The dissociation constant, K_d, of nSH3:PRM complexes was measured by monitoring the change of tryptophan fluorescence signal. Excitation wavelength was 295 nm. All binding assays were performed in a stirred 1-cm path-length cuvette using a QM-400 fluorimeter (Photon Technology International/HORIBA Scientific, Edison, NJ). Protein concentration used for the fluorescence-based binding assays was 0.1 μM. All measurements were done in 20 mM sodium phosphate (pH 6.1) and 80 mM NaCl. All of the experiments were repeated two or three times. K_d was calculated by assuming a 1:1 complex, and by the global fitting of the repeatedly measured fluorescence intensities to Eq. 1:

$$\Delta F = \Delta F_{\max}\left(\frac{[P_t]+[L_t]+K_d \pm \sqrt{([P_t]+[L_t]+K_d)^2-4[P_t][L_t]}}{2[P_t]}\right), \quad (1)$$

where ΔF and $\Delta F_{\max}$ are the signal change and the maximum amplitude of signal change, respectively. P_t is the total protein concentration and L_t is the total ligand concentration at each titration point.

Van 't Hoff analysis

The K_d values of the nSH3:PRM complexes were measured at seven different temperature points, from 10 to 40°C, using fluorescence-based method. The binding free energy, ΔG°, was calculated using $\Delta G^{\circ} = -RT\ln(K_d)$. Binding thermodynamic parameters, ΔH°, and ΔS°, were calculated by fitting the temperature-dependent ΔG° to Eq. 2 (32), with and without taking into account ΔC_p:

$$\Delta G^{\circ}_{\text{bind}}(T) = \Delta H^{\circ}_{\text{bind}}(298K) + \Delta C^{\circ}_p(T-298K) - T\left(\Delta S^{\circ}_{\text{bind}}(298K) + \Delta C^{\circ}_p \ln(T-298K)\right). \quad (2)$$

An extensive Monte Carlo simulation study indicated that the errors of ΔH° and ΔS° obtained from van 't Hoff analysis are proportional to the relative

error of K_d, and the use of symmetric temperature range around the standard temperature (25°C) was suggested to reduce the effect of the error of K_d on the thermodynamic parameters (33).

Crystallization, data collection, processing, and structure determination

Crystallization conditions were found after screening several commercial (Hampton Research, Aliso Viejo, CA) and in-house screens. 4 mM nSH3 was mixed with 5 mM PRM^{758} in a molar ratio of 1:1 and incubated for 30 min for the crystallization trials. The best diffracting crystals were obtained by sitting drop vapor diffusion method in 0.1 M sodium acetate trihydrate (pH 4.5), 13% polyethylene glycol 3350, 3.0 M sodium chloride. Crystals grew approximately to dimensions of 0.3 × 0.2 × 0.2 mm. A 1.8 Å resolution data set was collected at 113 K using an R-AXIS IV^{2+} imaging-plate detector and Cu $K\alpha$ radiation generated by a rotating-anode x-ray generator (Rigaku/MSC, The Woodlands, TX). The data were processed using HKL2000 (34) in space group $P12_11$ with cell dimensions of $a = 45.2$ Å, $b = 29.5$ Å, and $c = 45.8$ Å. The solution was subjected to an initial cycle of model rebuilding using AutoBuild module of PHENIX (35) followed by several iterations of manual model building in COOT (36) and refinement in REFMAC (37). PRM^{758} was added to both copies of the model guided by the F_o-F_c electron density map.

NMR spectroscopy

All NMR experiments were conducted using protein samples in 20 mM sodium phosphate (pH 6.1), 80 mM NaCl, 0.02% sodium azide, 1 mM EDTA, 10 μM DSS (4,4-dimethyl-4-silapentane-sulfonate), and 10% D_2O at 25°C. NMR spectra were acquired on an AVANCE 600 and 800 MHz spectrometers (Bruker, Billerica, MA), equipped with a cryogenic probe. NMR spectra were processed with NMRPipe (38) and analyzed with NMRViewJ (One Moon Scientific, Westfield, NJ) and CARA (39). The assignment of ^{1}H, ^{13}C, and ^{15}N resonances was carried out using a set of experiments: (^{1}H, ^{15}N) heteronuclear single quantum coherence, (^{1}H, ^{13}C) heteronuclear single quantum coherence, HNCO (40), HNCACB (41), HN(CO)CA (42), HNCA (43), HN(CA)CO (44), CBCA(CO)NH (45), HBHA(CO)NH (46), and HC(C)H-TOCSY (47). ^{1}H chemical shifts were referenced with respect to DSS, and ^{13}C and ^{15}N chemical shifts were referenced indirectly (48).

Measurement of relaxation parameters

All relaxation parameters were measured at 25°C on a 500 MHz NMR spectrometer (Bruker). For R_1, five relaxation time points were taken between 100 ms and 1 s. For R_2, five relaxation time points were taken between 4 and 120 ms. For R_1 and R_2 measurements, a recycle delay of 2 s was used between transitions. For the heteronuclear nuclear Overhauser effect measurements, a recycle delay of 10 s was used in reference experiment. The saturation of proton during steady state was performed by applying 180° pulses for 4 s (49). Errors of the relaxation parameters were estimated using duplicated measurements.

Model free analysis

The R_1, R_2, and heteronuclear nuclear Overhauser effect were analyzed according to the Lipari-Szabo model free formalism (50,51) using the softwares Modelfree version 4.20 (52) and FAST-Modelfree (53). An initial estimation of the rotational diffusion tensor of PRM-bound state was performed using the programs Quadratic and Pdbinertia (http://cpmcnet.columbia.edu/dept/gsas/biochem/labs/palmer/software.html). The axially symmetric diffusion tensor was used for analysis of the complex. The isotropic diffusion model was used for analysis of the free nSH3 domain. Anisotropic model was also tested but the isotropic model yielded lower sum of squared errors.

Structure-based calculation of thermodynamic parameters

Thermodynamic parameters were calculated based on the change of the solvent-accessible surface area (SASA), upon the complex formation of the nSH3 domain and PRM. The structure of free nSH3 domain (PDB: 1M30) and the crystal structures of nSH3:PRM^{758} complex (PDB: 5IH2) were used for the calculations. The changes in polar and nonpolar solvent-accessible surface area ($\Delta SASA_{\rm pol}$ and $\Delta SASA_{\rm np}$) were calculated using parameter-optimized surfaces web server (54,55). All water molecules were removed from PDB files before calculation. The effect of structured water molecules on the SASA was calculated after adding the identified water molecules to the PDB file. The structured water molecules were considered absent from the free nSH3 domain.

Heat capacity change upon complexation, ΔC_p, was calculated by the Eq. 3 using the estimated $\Delta SASA_{\rm pol}$ and $\Delta SASA_{\rm np}$ (56):

$$\Delta C_p^\circ = a\Delta SASA_{np} + b\Delta SASA_{\rm pol}, \quad (3)$$

where $a = 0.45$ cal K^{-1} $(Å^2)^{-1}$ and $b = -0.26$ cal K^{-1} $(Å^2)^{-1}$. The enthalpy change according to $\Delta SASA_{\rm pol}$ and $\Delta SASA_{\rm np}$ was parameterized at 60°C, which is the midpoint of thermal unfolding of proteins. The enthalpy change, ΔH (60°C), was calculated using Eq. 4 (28):

$$\Delta H^\circ_{\rm bind}(60^\circ C) = a(60)\Delta SASA_{\rm pol} - b(60)\Delta SASA_{np} + \Delta H_{\rm ion}, \quad (4)$$

where $a(60)$ and $b(60)$ are the empirical coefficients obtained from the regression analysis of protein thermal unfolding data set, and 31.4 cal $(\text{mol Å}^2)^{-1}$ and −8.44 cal $(\text{mol Å}^2)^{-1}$, respectively. The empirical parameterization of the binding enthalpy for protein-ligand interaction at 25°C resulted in Eq. 5 (57):

$$\Delta H^\circ_{\rm bind}(25^\circ{\rm C}) = \Delta H_{\rm conf}(25^\circ{\rm C}) + a(25)\Delta SASA_{np} + b(25)\Delta SASA_{\rm pol}, \quad (5)$$

where $a(25) = -7.35$ cal $(\text{mol Å}^2)^{-1}$ and $b(25) = 31.06$ cal $(\text{mol Å}^2)^{-1}$, and $\Delta H_{\rm conf}$ represents the enthalpy change accompanied by the conformational change of protein and ligand upon binding. The entropy change of solvent, $\Delta S^\circ_{\rm solv}$, associated with the burial of hydrophobic surface after binding at a temperature T was calculated using the Eq. 6 (56):

$$\Delta S^\circ_{\rm solv} = -0.26\Delta SASA_{\rm pol}\ln\left(\frac{298}{T_{\rm pol}}\right) + 0.45\Delta SASA_{np}\ln\left(\frac{298}{T_{np}}\right), \quad (6)$$

where $T_{\rm pol} = 335.15$ K and $T_{\rm np} = 385.15$ K are the polar and nonpolar reference temperatures at which the hydration entropy is equal to zero (28,56).

RESULTS AND DISCUSSION

Identification of Crk binding sites in Abl kinase

The C-terminal disordered region (from amino acid 512–1130 in Abl-1A) of cAbl contains seven PxxP motifs

(Table S1 in the Supporting Material). In this study, we have investigated the binding of the nSH3 domain to all individual PRMs. We have tested seven PRMs and found that the nSH3 domain binds to three of them (Table 1 and Table S1). The amino-acid sequences of the PRMs that bind to the nSH3 domain are shown in Table 1. The number in a peptide name represents the amino-acid number of the first proline in PxxP motif in Abl-1A sequence. The binding between $nSH3^{CrkII}$ and PRMs was measured by monitoring the changes in tryptophan fluorescence intensity of the nSH3 domain (Fig. 1). The three nSH3:PRM complexes have similar K_d values, on the order of 1–2 μM. The affinities of the three peptides for $nSH3^{CrkII}$ are comparable to the affinity of PRM^{524} to CrkL (58). All three binding peptides have a common PxφPxK motif. Intriguingly, we did not observe the binding of nSH3 to PRM^{610}, although it contains the PxxPxR motif. Similarly, the binding of nSH3 and PRM^{610} was identified by phage display screening, but it was not detected by GST-pulldown assay (22). The interaction between the nSH3 and PRM^{758} was confirmed unambiguously in our study. The functional significance of nSH3:PRM^{758} interaction was confirmed by the results showing that the deletion of two PRMs (PRM^{524} and PRM^{568}) does not inhibit the phosphorylation of Crk by cAbl kinase (24).

The structure determination of nSH3:PRM^{758} complex

We have determined the crystal structure of the nSH3:PRM^{758} complex (Fig. 2) at 1.8 Å resolution (Table S2). The complex crystallizes in the space group $P12_11$ with cell dimensions of a = 45.2 Å, b = 29.5 Å, and c = 45.8 Å. Molecular replacement in Phaser (59) using nSH3 domain (PDB: 1CKA) (12) as a search model could output a unique solution. The solution contained two copies of the protein in the asymmetric unit. A Matthews coefficient (V_M) of 2.18 for two copies of the protein also indicated the same. Water molecules were added after one more round of real and reciprocal space refinement. The final structure has R/R_{free} = 17%/24%.

We adopted the notation where φ in PxφPxK motif is designated as P_0 position (φ represents hydrophobic residues) (60). The residues located at the C-terminal end of P_0 were designated as P_{-1}, P_{-2}, etc. The residues located at the N-terminal of P_0 were designated as P_1, P_2, etc. In that complex, the side chains of Y_5, E_4, A_1, and R_{-2} of PRM^{758} do not interact directly with the nSH3 domain. The hydrophobic binding interface of the complex is formed by P_2, L_0, and P_{-1} in the PRM, and F141, F143, W169, P183, P185, and Y186 in the nSH3 domain. A salt-bridge network was observed between K_{-3} in PRM and a cluster of acidic residues (D147, E149, and D150) in the RT-loop of the nSH3 domain (Fig. 2). This salt-bridge network is critical for the binding affinity and the recognition of specific PRMs (12).

Two molecules per asymmetric unit were observed, and although these two complex molecules are highly similar (average Cα RMSD = 0.4 Å), the conformations of RT-loop and nSrc-loop show considerable difference from each other (Fig. 2). These loops are crucial for the recognition of a specific PRM sequence (12,60). This structural heterogeneity is due to the low packing density in these parts of the molecule: the contacts between the nSH3 domain and PRM represent salt-bridge interactions between the terminal charged groups of long side chains. The similar dynamic behavior of RT-loop was suggested by a thorough analysis using molecular dynamics simulation of the complex between the nSH3 domain and PRM derived from SOS protein (61).

To gain structural insights into two other nSH3:PRM^{cAbl} complexes, we conducted NMR CSP analysis (Fig. 3). Three peaks corresponding to the E149, D150, and W169 show significantly large CSPs, compared to others. Because large CSPs of these three residues considerably affect the overall mean and standard deviation, we did not include the CSPs of these residues for the calculation of CSP statistics. Then, the residues showing the CSP larger than the sum of the mean and standard deviation are identified, and the excluded residues were added afterwards. Fig. 3 shows the identified residues for each complex.

Despite overall similarity, the magnitudes of CSPs of the complexes differ considerably among each other. Fig. 3 *D* shows the standard deviation of the CSPs from these three complexes. The residues showing standard deviations larger than the average value are mapped on the binding interface (Fig. 4). This reflects the variability of amino-acid sequences in the bound PRMs. The CSPs of E149 and D150 show the largest standard deviations. These residues form a salt-bridge network with the K_{-3} of bound PRM (Fig. 2 *A*). This may indicate considerable structural heterogeneity of the salt-bridge interactions in different complexes, and this is consistent with the structural variation in the same region between the two complex structures in the asymmetric unit, as well.

TABLE 1 The Thermodynamic Parameters for the Interactions between the nSH3 Domain and PRMs: T = 298 K

Peptides	K_d (μM)	ΔG° (kcal mol^{-1})	ΔH° (kcal mol^{-1})	$-T\Delta S^\circ$ (kcal mol^{-1})
PRM^{524} QAPELPTKTRTSY	1.72 ± 0.47	−7.86 ± 0.45	−15.37 ± 0.31	7.51 ± 0.32
PRM^{568} VSPLLPRKERGY	2.90 ± 0.19	−7.55 ± 0.99	−16.78 ± 0.70	9.23 ± 0.70
PRM^{758} YEKPALPRKR	1.72 ± 0.48	−7.86 ± 0.44	−11.50 ± 0.31	3.64 ± 0.31

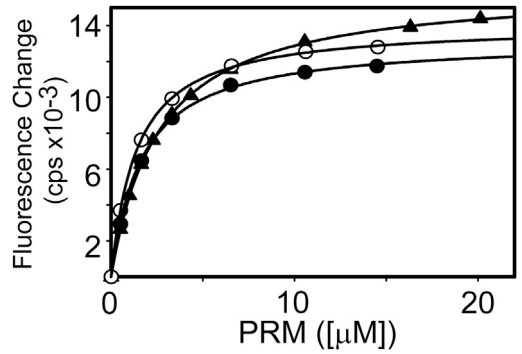

FIGURE 1 Binding isotherms of the nSH3 domain to PRM^{524} (*solid circles*), PRM^{568} (*triangles*), and PRM^{758} (*open circles*) of cAbl.

Thermodynamic characterization of ligand binding to nSH3 domain

To measure the thermodynamic parameters (ΔH° and ΔS°) associated with the binding of nSH3 and PRMs, we conducted van 't Hoff analysis. When properly executed, there is no systematic difference between the thermodynamic parameters obtained by van 't Hoff analysis and calorimetric measurement (62). The K_d values of the nSH3:PRM^{cAbl} complexes were measured using fluorescence spectroscopy as a function of temperature ranging from 10 to 40°C (Fig. 5). Thermodynamic parameters are reported in Table 1. As described in Materials and Methods, our experimental temperature range is symmetrical, with respect to the standard state temperature (25°C). This also helps reduce the error of ΔH° and ΔS° estimated by van 't Hoff analysis.

The results of the van 't Hoff analysis indicate that the binding of nSH3 and all three PRMs is driven by favorable enthalpy, accompanied by unfavorable entropy changes at 298 K (Table 1). The obtained ΔH° and ΔS° for all three complexes are within the typical range for SH3:PRM interactions (30). Although the binding free energies of all three complexes are similar to each other, ΔH° and $-T\Delta S^\circ$ vary considerably. ΔH° and $-T\Delta S^\circ$ of nSH3:PRM^{758} binding is notably smaller than for the other two complexes. This is especially interesting because all three PRMs contain the identical core sequences (PxLPxK), and the other residues in the PRM do not interact with nSH3 domain.

Because PRMs form type-II polyproline (PPII) helix in the complex, we further investigated whether the difference in the PPII helix propensities of PRMs can explain the differences in binding thermodynamic parameters of the three nSH3:PRM complexes. To calculate the PPII propensity of each PRM, we simply summed up the propensities of individual constituent amino acids, determined by various methods (63–65). We have not found a correlation between the calculated PPII propensity of $PRMs^{cAbl}$ and any of the thermodynamic parameters. The absence of correlation between PPII propensity and thermodynamic parameters has been observed for other SH3:PRM interactions (66–68). However, the effect of PPII propensity to binding thermodynamics was shown in the binding of PRM^{Sos} to Sem-5 cSH3 domain (69,70). Because we tested only three PRMs in this study, the effect of PPII helix propensity on binding affinity should be further tested with a larger data set.

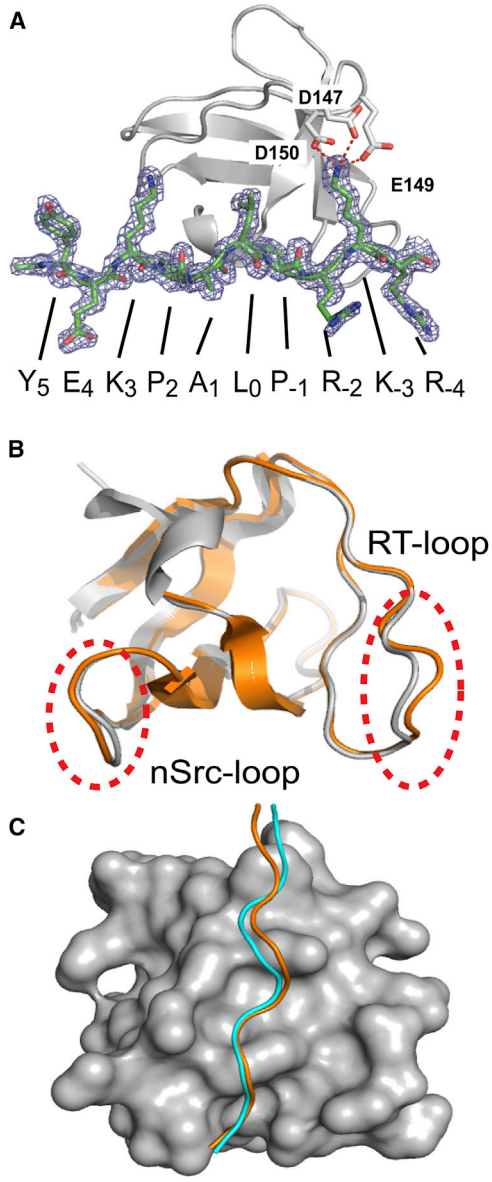

FIGURE 2 The structure of the nSH3:PRM^{758} complex. (*A*) Representation of the 2Fo-Fc electron density map of PRM^{758} contoured at 1σ. The amino-acid sequence of PRM^{758} is shown at the bottom. Salt-bridges between K_{-3} of PRM^{758} and three acidic residues (D147, E149, and D150) of the nSH3 domain are shown in red. Salt-bridges between the acidic residues in nSH3 domain and K^{-3} of PRM^{758} are shown as dashed lines. Overlaid structures of (*B*) two nSH3 domains (*gray* and *orange* for molecules A and B in the PDB file, respectively) and (*C*) bound PRMs in an asymmetric unit of the nSH3:PRM^{758} complex crystal. PRMs bound to molecules A and B are shown in cyan and orange color, respectively. To see this figure in color, go online.

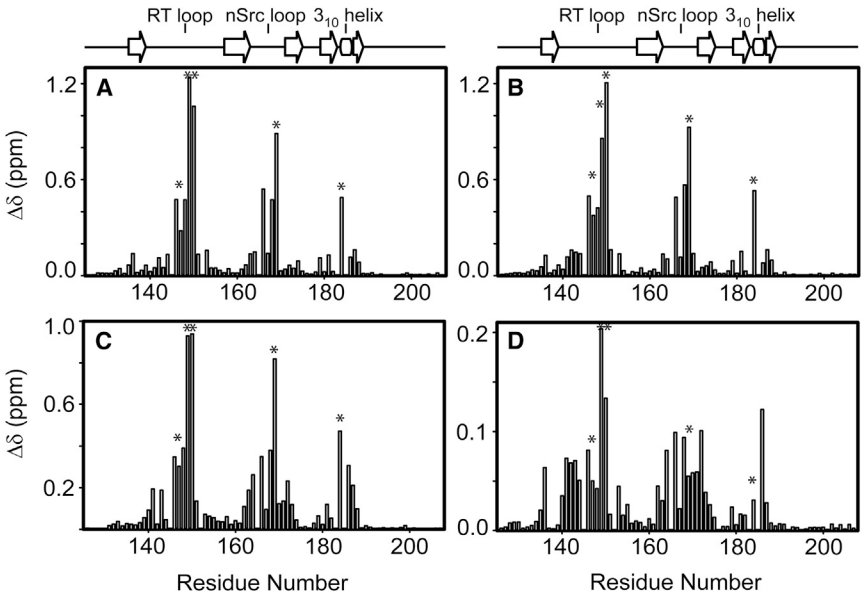

FIGURE 3 NMR CSP plots of backbone amide resonances of the nSH3 domain upon binding to (*A*) PRM^{524}, (*B*) PRM^{568}, and (*C*) PRM^{758}. (*D*) Standard deviation of NMR CSPs of the three complexes. Key binding interfacial residues (D147, E149, D150, D169, and Y184) are marked by the * symbol.

Structure-based calculations of thermodynamic parameters

Because of the hydrophobic binding interface, the binding of the SH3 domain and PRM is associated with a change in the heat capacity (ΔC_p), which leads to the appearance of nonlinear curve in the van 't Hoff plot. Therefore, the change in ΔC_p can be obtained by measuring the nonlinearity of van 't Hoff plot. Although the fitting with nonlinear model (Eq. 2) provides a smaller sum of squared errors compared to a linear model, the improvement of the fit was not statistically significant, based on the F-test with $\alpha = 0.05$. Table 1 shows the results of the application of the simple linear model (i.e., $\Delta C_p = 0$).

We further investigated why the van 't Hoff plot of the nSH3:PRM^{cAbl} interaction does not show the curvature, despite the hydrophobic binding interface shown in the analysis of crystal structure. The changes in solvent-accessible surface ($\Delta SASA$) are associated with protein-ligand interaction, which is a major source of the heat capacity change (28,57). Therefore, we first tested whether the results obtained by van 't Hoff analysis are consistent with the change in $\Delta SASA$ upon the nSH3:PRM complexation. We measured the change in polar and nonpolar solvent-accessible surface area, $\Delta SASA_{pol}$ and $\Delta SASA_{np}$, between NMR-derived structure of free nSH3 and the crystal structure of nSH3:PRM^{758} complex. SASA was calculated by taking the average of all structures in each PDB file. Applying $\Delta SASA$ to Eq. 3, we determined that $\Delta C_p = -204.6$ cal mol^{-1} K^{-1}. We fit van 't Hoff plot with this calculated ΔC_p as a restraint. While the regression curve displayed the curvature, the fitted values of ΔH° and $\Delta \mathbf{S}^\circ$ were virtually identical to the values obtained by linear van 't Hoff equation. A similar result was obtained when we applied a different $\Delta C_p = -255.4$ cal mol^{-1} K^{-1}, which is calculated based on the $\Delta SASA$ estimated by the crystal structure in the presence and absence of PRM. The calculated ΔC_p values are also similar to the experimentally determined values for different SH3:PRM interactions (27,28). For example, a negative $\Delta C_p = -166$ cal mol^{-1} K^{-1}, was obtained for the interaction of Sem-5 SH3 and

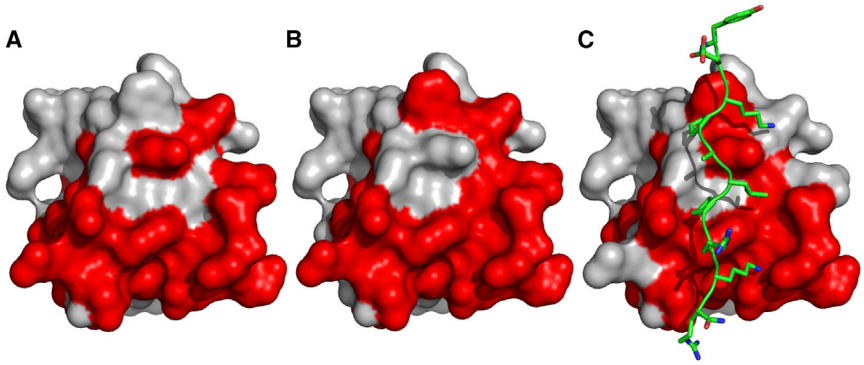

FIGURE 4 Mapping of binding interfaces between the nSH3 domain and PRMs. Significant NMR CSPs upon binding of (*A*) PRM^{524}, (*B*) PRM^{568}, and (*C*) PRM^{758} are shown in red. The structure of PRM^{758} is shown in (*C*). To see this figure in color, go online.

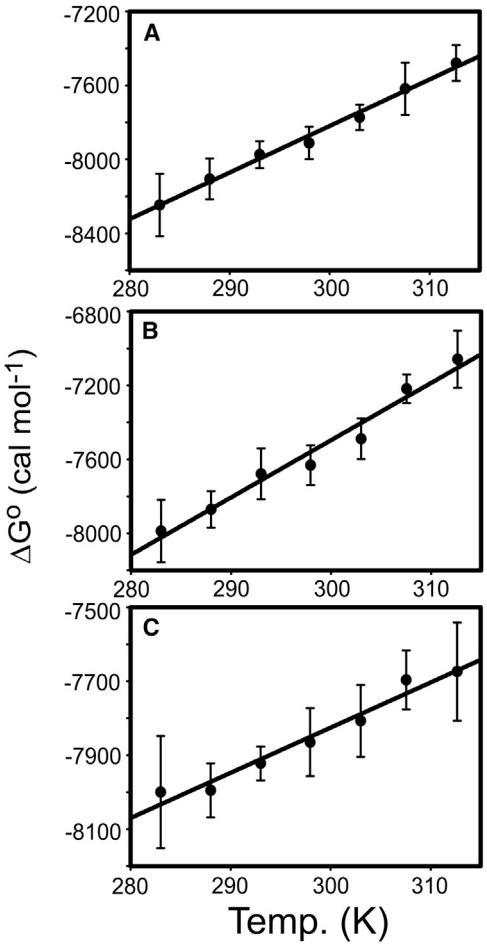

FIGURE 5 Van 't Hoff plots of the interactions between the nSH3 domain and (*A*) PRM^{524}, (*B*) PRM^{568}, and (*C*) PRM^{758}. The lines are linear regression fits using Eq. 2 with $\Delta C_p = 0$.

PRM (28). Taken together, these results indicate that ΔSASA, upon the binding of nSH3 domain and PRM, is too small for nonlinear van 't Hoff plot to be observed in the investigated temperature range (from 283 to 310 K). However, due to the concern of protein stability at higher temperatures, we did not extend our temperature range. This test also implies that the measured enthalpy and entropy values for the nSH3:PRM^{cAbl} are reliable.

Molecular origin of the anomalous thermodynamic parameters

Understanding the molecular origin of thermodynamic parameters is one of the major goals in molecular biophysics and it is important for the rational ligand design as well. However, the calculations of the thermodynamic parameters of SH3:PRM interactions have generally resulted in serious inconsistency with experimental outcomes. Therefore, we sought to identify the molecular basis of the discrepancy between the experimental and the calculated results.

We first calculated the binding enthalpy, ΔH°_{bind}, based on the structural change using Eq. 4. However, we found that the use of this equation yields ΔH°_{bind} values that significantly deviate from the experimental result, regardless of our choice of coefficients. For example, when $a = -8.43$ and $b = 31.06$ are applied, this calculation yields $\Delta H^\circ_{bind} = 4.7$ kcal mol^{-1}, which is drastically different from the experimental value ($\Delta H^\circ_{bind} = -11.5$ kcal mol^{-1}). The choice of free nSH3 domain structure can affect the calculated ΔH°_{bind} because of the structural rearrangements upon the complexation. Here, however, the calculation of $\Delta SASA_{pol}$ and $\Delta SASA_{np}$ using crystal structure, with and without bound ligand, yielded similar results as when NMR and crystal structures were used as a model for free and PRM-bound states, respectively. It should be noted that this result does not indicate that the nSH3 domain undergoes minor structural changes upon binding to ligand. Instead, it indicates that the structural change does not result in considerable SASA changes. The selection of a different free nSH3 structure from 20 lowest-energy NMR structures results in a larger change in SASA. To avoid any bias stemming from the selection of a specific free nSH3 structure, we simply used the average value of all available free nSH3 structures.

The change in protonation state of protein and ligand can affect ΔH°_{bind}. However, the detailed studies of several other SH3:PRM interactions showed that this effect is typically minor (27,28). To further test the effects of ionization on ΔH°_{bind}, we measured the K_d of nSH3:PRM^{758}, at pH 7.5 in HEPES buffer (Fig. S1 in the Supporting Material). The obtained K_d value was shown to be very similar to the results of our choice of experimental conditions in this study: phosphate buffer at pH 6.1. Although further tests are necessary, this result supports our assumption that ΔH°_{ion} does not contribute greatly to the difference between the experimental and theoretical ΔH°_{bind}.

Next, we tested whether the observed difference is due to fact that these coefficients are derived from protein (un) folding data, and not from protein-ligand binding data. Luque and Freire (57) reparameterized the coefficients based on the binding data of HIV-1 protease and inhibitors at 25°C. When we applied Eq. 5, the calculation yielded $\Delta H^\circ_{bind} = -3.42$ kcal mol^{-1}, which is much closer to the experimental value. This improvement might be due to the relatively smaller binding interface of SH3:PRM complex compared to $\Delta SASA$ associated with protein (un)folding process.

Water molecules at the binding interface of nSH3 and PRM

There is a growing interest in the role of water molecules at the binding interface of protein and ligand in the binding thermodynamics (31,71–73). It has been suggested that an incomplete dehydration of binding interface can result in considerable favorable enthalpy and unfavorable entropy

changes (57,74). Therefore, the atypical ΔH° and $-T\Delta S^{\circ}$ of nSH3:PRM interaction can be attributed to the water molecules located at the binding interface. Recent studies indicated that the binding interfaces of many SH3:PRM complexes include structured interfacial water molecules (31,72,75). The localization of water molecules was identified in three regions, including the 3_{10}-helix, nSrc-loop, and RT-loop regions (75). The enthalpy contribution of water molecules in the 3_{10}-helix region of $SH3^{cAbl}$:PRM^{p41} complex was estimated to be –4.78 kcal mol^{-1} (27).

We investigated whether interfacial water molecules are responsible for the discrepancy between the experimental and calculated thermodynamic parameters of $nSH3:PRM^{cAbl}$ interactions. We compared $nSH3^{CrkII}$:PRM^{758} structure with $SH3^{cAbl}$:PRM^{p41} complex, where five specific interfacial water molecules were identified. However, $nSH3:PRM^{758}$ complex does not contain water molecules at the sites identified in $SH3^{cAbl}$:PRM^{p41} complex. Only one interfacial water molecule in $nSH3:PRM^{758}$ is located at a similar site in the nSrc loop region, but this water site is characterized as a transient binding site, and it underwent fast exchange with bulk water in the molecular dynamic simulation of $SH3^{cAbl}$:PRM^{p41} complex (75).

Furthermore, we searched for a set of interfacial water molecules, conserved specifically in the nSH3:PRM complexes. Because of the diversity of amino-acid sequences and the structures of SH3:PRM interfaces, it is not unreasonable to expect that there are interfacial water sites unique to each SH3 domain. To identify the conserved interfacial water molecules, we superimposed all available crystal structures of nSH3:PRM complexes (PDB: 1CKA, 1CKB, and 5IH2). We found eight water molecules that are located at very similar sites in all three complexes. Additionally, we identified several more water molecules per complex that mediate the interactions between the bound ligand and the nSH3 domain. However, only a small number of interfacial water molecules in each complex showed the characteristics of buried water molecules that might affect binding energetics: i.e., low normalized B-factors (<0.4 $Å^2$) and SASA (<10 $Å^2$) (76). Consequently, we identified two water molecules (w34 and w53) that are conserved in all nSH3:PRM complexes and have low normalized B-factor and SASA values (Fig. 6).

To estimate the effects of the two interfacial water molecules on the binding thermodynamics, we recalculated $\Delta SASA$ taking into consideration the interfacial water molecules as a part of bound ligand. This resulted in the increase of $\Delta SASA_{pol}$ by ~200 $Å^2$ upon the complexation. The calculation based on this $\Delta SASA$ resulted in $\Delta H^{\circ}_{bind} = -9.4$ kcal mol^{-1}, which is a significant improvement compared to the result obtained without considering the water molecules. The increase in $\Delta SASA_{pol}$ improved the agreement between the calculations and the experimental results, regardless of the choice of the coefficients and equations. This result indicates that the interfacial water can contribute considerably to the binding thermodynamics. However, it should be noted that these water molecules have higher B-factors than well-buried water. Therefore, the validity of these water molecules as buried (or structured) remains to be further investigated. We speculate that our results represent the upper bound of the contribution of interfacial water in nSH3:PRM complex.

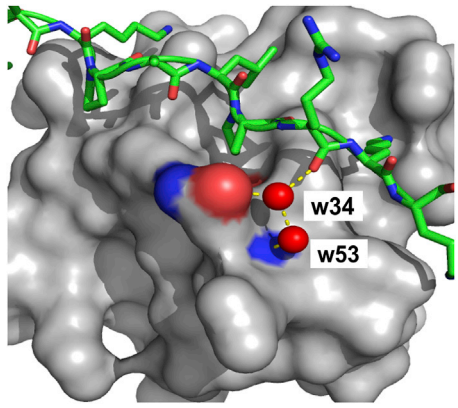

FIGURE 6 Water molecules at the $nSH3:PRM^{758}$ binding interface. The nSH3 domain is shown as a surface representation. Two water molecules (w34 and w53) are hydrogen-bonded with the side-chain and backbone amides of Q168, respectively, in the nSH3 domain and mediate the interactions with the backbone carbonyl oxygen of R_{-2} in PRM^{758}. To see this figure in color, go online.

Role of conformational entropy in nSH3:PRM interaction

In the calculation of ΔH°_{bind} we ignored ΔH°_{conf}, which represents the structural rearrangement of protein and ligand upon complexation. This suggests that the difference between experimental and calculated ΔH°_{bind} can be due to conformational rearrangement of protein and ligand. It was shown that the ΔH°_{conf}, obtained as a fitting parameter of Eq. 5 to several protein-ligand binding data, ranges from 0.1 to 5.9 kcal mol^{-1} (57). However, most of the ligands used in the calculations are small molecules. For ~10 amino-acid-long peptides used in this study, ΔH°_{conf} could be considerably larger than the reported values. In addition, the effect of conformational flexibility on the estimation of binding thermodynamic parameters was well highlighted in the study of the Sem-5 cSH3 domain (77,78).

We have estimated the contribution of the conformational entropy, $-T\Delta S^{\circ}_{conf}$, accompanied by the rearrangement of protein and ligand, to the binding thermodynamic parameters. The two major components of binding entropy change are the conformational entropy of protein and ligand, and solvent (or solvation) entropy ($\Delta S_{bind} = \Delta S_{conf} + \Delta S_{solv}$). Therefore, if we compare the $-T\Delta S_{bind}$ and $-T\Delta S_{solv}$, we can indirectly estimate $-T\Delta S_{conf}$. We first calculated the solvent entropy change upon the $nSH3:PRM^{758}$ interaction, using Eq. 6. The calculated $-T\Delta S_{solv}$ was –15.8 kcal mol^{-1} at

298 K, and differed by >18.0 kcal mol^{-1} compared to the experimentally obtained binding entropy change. Furthermore, the sign of the calculated $-T\Delta S_{solv}$ is opposite to $-T\Delta S_{bind}$. A considerable difference between $-T\Delta S_{bind}$ and calculated $-T\Delta S_{solv}$ was also observed for other SH3:PRM interactions (27,28). These results indicate that the conformational entropy change contributes significantly to $-T\Delta S_{bind}$, and consequently to the overall binding thermodynamics. It is also important to point out that our estimation of $-T\Delta S_{solv}$ does not take into account the interfacial water molecules. $-T\Delta S_{conf}$ associated with the ordering of a water molecule was estimated to be on the order of 2 kcal mol^{-1} at 298 K (74). Therefore, the interfacial water can considerably affect the estimation of $-T\Delta S_{solv}$, but this does not affect our conclusion that conformational entropy contributes significantly to the binding thermodynamics of nSH3 and PRM.

NMR dynamic studies provided a quantitative estimation of conformational entropy contribution (79–81). To further determine the contribution of conformational entropy to the binding thermodynamics, we have measured backbone N-H bond order parameters (O^2) of the nSH3 domain in free and PRM^{758}-bound states, using the Lipari-Szabo model-free approach (50,51). Although structural change upon PRM-binding is mainly localized in nSrc- and RT-loops, PRM-induced changes in O^2 are observed beyond the ligand binding interface (Fig. 7 *A*). These results may indicate that favorable binding energy is redistributed to optimize overall backbone hydrogen-bond geometry of SH3 domain as observed for other SH3:PRM interactions (29,82).

The change in O^2 values upon ligand-binding can be converted to the change in $T\Delta S_{conf}$ of individual N-H bonds (Fig. 7 *B*) (79,80). The sum of all individual NMR-derived $T\Delta S_{conf}$ yields −4.79 kcal mol^{-1} at 298 K. Similarly, the binding of PRM to the Src SH3 domain resulted in conformational entropy change by –1.5 ± 0.6 kcal mol^{-1} (29). Here, we excluded the flexible N- (residues 126–133) and C-terminal (residues 190–207) tails. In addition, we did not take into account the change in motions in timescales slower than the overall tumbling time of protein molecule. Although this calculation has some limitations, the result clearly indicates that the conformational entropy contributes significantly to overall binding entropy. A large portion of $-T\Delta S_{solv}$ is compromised by ordering backbone N-H bonds in the nSH3 domain. The sum of ΔS_{solv} and ΔS_{conf} is still considerably different from the ΔS_{bind}. However, it should be emphasized that here we only considered backbone N-H bonds of the nSH3 domain. The folding of the disordered PRM to PPII conformation upon binding contributes substantially to the conformational entropy change. A remarkable example of this is the energetic contribution of conformational change of PRM upon binding to the Sem-5 SH3 domain (28). The authors found that the thermodynamic signature corresponding to the formation of PPII helix by PRM^{Sos} is similar to the difference between the

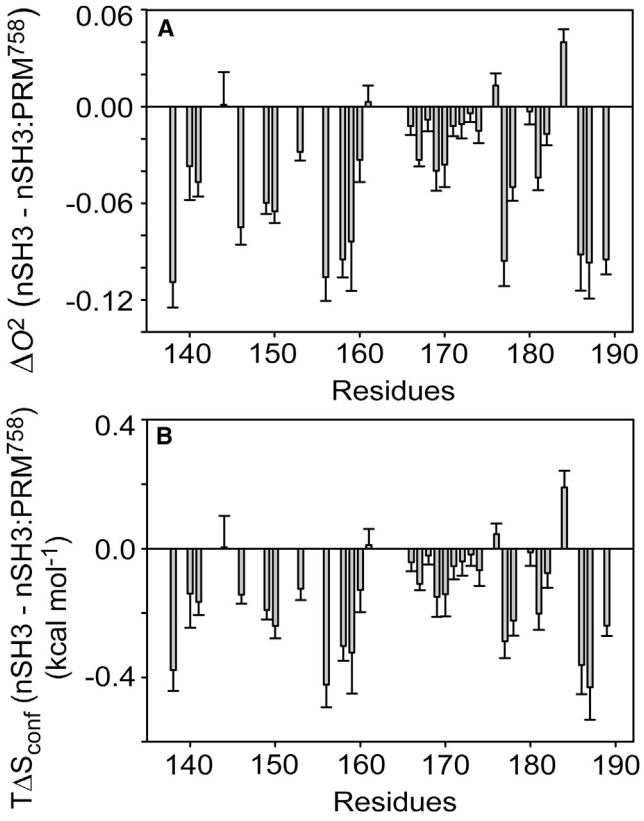

FIGURE 7 (*A*) Difference of backbone N-H order parameters (O^2) between the free and PRM-bound nSH3 domains. (*B*) Conformational entropy change of N-H bonds in the nSH3 domain upon binding of PRM^{758} (T = 298 K).

experimental and calculated thermodynamics based on static structures. Furthermore, the change in side-chain motion upon complexation contributes considerably to this as well (83).

In this study, we observed that the binding thermodynamics of the nSH3:PRMs^{cAbl} complexes differ considerably, despite the fact that they have similar binding interfaces. It is noteworthy that Ferreon et al. (77) and Manson et al. (78) demonstrated that the conformational fluctuation of RT-loop can affect the binding thermodynamics between the cSH3^{Sem5} domain and PRM^{Sos} considerably. Hence, it raises the possibility that the difference in the binding thermodynamics among the nSH3:PRMs^{cAbl} complexes is due to the differences in the conformational heterogeneity between the complexes. Furthermore, it is equally possible that the differences in the conformational dynamics among the PRMs^{cAbl} are responsible for the difference in binding thermodynamics.

Biological implication of nSH3^{CrkII}:PRM^{cAbl} interactions

We have examined the binding of the nSH3 domain of CrkII to all putative binding PRMs in cAbl. Our study shows that

three PRMs in cAbl mediate the interactions with CrkII. It remains unknown why cAbl contains multiple PRMs for CrkII interactions. While the interaction of CrkII and cAbl results in the phosphorylation of CrkII, the deletion of two PRMs (PRM^{524} and PRM^{568}) does not inhibit the phosphorylation of Crk by cAbl kinase (24). This indicates that a single PRM may be enough to induce the phosphorylation of CrkII. It may possible that the binding of CrkII to each of the PRMs in cAbl enables different biological roles.

Signaling adapters containing SH3 domain, such as CrkII, Grb, and Nck, bind to these PRMs in cAbl (20,22). For example, Grb2 can bind to PRM^{524} and PRM^{568} (20), and Nck binds to PRM^{610} (20,22). This raises the possibility that these adaptor proteins bind simultaneously to cAbl. In light of these results, Antoku et al. (22) proposed an interesting model in which the binding of CrkII to multiple PRMs regulates the binding of other proteins to cAbl. For example, it was suggested that the binding competition of CrkII and Nck for the PRMs in cAbl regulates cell spreading (22). Although the C-terminal region of cAbl contains three nuclear localization signals, it is not exclusively localized to the nucleus (84), and the PRMs are located near nuclear localization signal sites. This suggests that CrkII binding may block the translocation of cAbl to the nucleus (20). In fact, PRM^{758} overlaps with nuclear localization signal (LPRKRAGE). Some PRMs in cAbl overlap with phosphorylation sites. The investigations of the functional relationship between PRM-mediated interactions and posttranslational modifications are of great importance.

CONCLUSIONS

In this study, we have investigated structures and thermodynamics of the interactions mediated by nSH3 domain of CrkII and PRMs of cAbl kinase. Understanding the molecular basis of the nSH3:PRM interaction is pivotal to successful design of small molecules that inhibit the interaction between CrkII and cAbl kinase. Despite its importance, binding free energy alone does not provide an insight into the mechanism by which protein-ligand interactions are achieved. Mechanistic insight into protein-ligand interaction requires the understanding of principles underlying the thermodynamic signatures of protein-ligand interactions. Our results, obtained by combination of structural, thermodynamic, and conformational dynamics analysis, highlight the role of interfacial water molecules and the conformational entropy in the SH3:PRM interactions. PRMs are one of the most abundant motifs of the eukaryotic proteome (85). Therefore, it is important to elucidate the mechanism underlying the selectivity of SH3:PRM-mediated protein-protein interactions. We expect that the results from this study will be useful to identify the mechanism underlying the ligand-selectivity of SH3 domains.

SUPPORTING MATERIAL

One figure and two tables are available at http://www.biophysj.org/biophysj/supplemental/S0006-3495(16)30285-5.

AUTHOR CONTRIBUTIONS

V.S.B. and J.-H.C. conceived the research; V.S.B., D.Z., I.K., and J.-H.C. conducted experiments; V.S.B., D.Z., I.K., J.C.S., and J.-H.C. analyzed data; and J.-H.C. wrote the article.

ACKNOWLEDGMENTS

Work in the J.-H.C. lab was supported by start-up funds from Texas A&M University.

SUPPORTING CITATIONS

Reference (86) appears in the Supporting Material.

REFERENCES

1. Mayer, B. J., M. Hamaguchi, and H. Hanafusa. 1988. A novel viral oncogene with structural similarity to phospholipase C. *Nature.* 332:272–275.
2. Matsuda, M., S. Tanaka, …, M. Shibuya. 1992. Two species of human CRK cDNA encode proteins with distinct biological activities. *Mol. Cell. Biol.* 12:3482–3489.
3. ten Hoeve, J., C. Morris, …, J. Groffen. 1993. Isolation and chromosomal localization of CRKL, a human crk-like gene. *Oncogene.* 8:2469–2474.
4. Prosser, S., E. Sorokina, …, A. Sorokin. 2003. CrkIII: a novel and biologically distinct member of the Crk family of adaptor proteins. *Oncogene.* 22:4799–4806.
5. Miller, C. T., G. Chen, …, D. G. Beer. 2003. Increased C-CRK proto-oncogene expression is associated with an aggressive phenotype in lung adenocarcinomas. *Oncogene.* 22:7950–7957.
6. Rodrigues, S. P., K. E. Fathers, …, M. Park. 2005. CrkI and CrkII function as key signaling integrators for migration and invasion of cancer cells. *Mol. Cancer Res.* 3:183–194.
7. Linghu, H., M. Tsuda, …, S. Tanaka. 2006. Involvement of adaptor protein Crk in malignant feature of human ovarian cancer cell line MCAS. *Oncogene.* 25:3547–3556.
8. Fathers, K. E., E. S. Bell, …, M. Park. 2012. Crk adaptor proteins act as key signaling integrators for breast tumorigenesis. *Breast Cancer Res.* 14:R74.
9. Sriram, G., and R. B. Birge. 2010. Emerging roles for crk in human cancer. *Genes Cancer.* 1:1132–1139.
10. Feller, S. M. 2001. Crk family adaptors-signalling complex formation and biological roles. *Oncogene.* 20:6348–6371.
11. Birge, R. B., C. Kalodimos, …, S. Tanaka. 2009. Crk and CrkL adaptor proteins: networks for physiological and pathological signaling. *Cell Commun. Signal.* 7:13.
12. Wu, X., B. Knudsen, …, J. Kuriyan. 1995. Structural basis for the specific interaction of lysine-containing proline-rich peptides with the N-terminal SH3 domain of c-Crk. *Structure.* 3:215–226.
13. Birge, R. B., J. E. Fajardo, …, H. Hanafusa. 1993. Identification and characterization of a high-affinity interaction between v-Crk and tyrosine-phosphorylated paxillin in CT10-transformed fibroblasts. *Mol. Cell. Biol.* 13:4648–4656.
14. Oda, T., C. Heaney, …, B. J. Druker. 1994. Crkl is the major tyrosine-phosphorylated protein in neutrophils from patients with chronic myelogenous leukemia. *J. Biol. Chem.* 269:22925–22928.

15. Matsuda, M., S. Ota, …, T. Kurata. 1996. Interaction between the amino-terminal SH3 domain of CRK and its natural target proteins. *J. Biol. Chem.* 271:14468–14472.

16. Tanaka, S., T. Morishita, …, K. Nagashima. 1994. C3G, a guanine nucleotide-releasing protein expressed ubiquitously, binds to the Src homology 3 domains of CRK and GRB2/ASH proteins. *Proc. Natl. Acad. Sci. USA.* 91:3443–3447.

17. Hasegawa, H., E. Kiyokawa, …, M. Matsuda. 1996. DOCK180, a major CRK-binding protein, alters cell morphology upon translocation to the cell membrane. *Mol. Cell. Biol.* 16:1770–1776.

18. Brehme, M., O. Hantschel, …, G. Superti-Furga. 2009. Charting the molecular network of the drug target Bcr-Abl. *Proc. Natl. Acad. Sci. USA.* 106:7414–7419.

19. Feller, S. M., B. Knudsen, and H. Hanafusa. 1994. c-Abl kinase regulates the protein binding activity of c-Crk. *EMBO J.* 13:2341–2351.

20. Ren, R., Z. S. Ye, and D. Baltimore. 1994. Abl protein-tyrosine kinase selects the Crk adapter as a substrate using SH3-binding sites. *Genes Dev.* 8:783–795.

21. Hantschel, O., and G. Superti-Furga. 2004. Regulation of the c-Abl and Bcr-Abl tyrosine kinases. *Nat. Rev. Mol. Cell Biol.* 5:33–44.

22. Antoku, S., K. Saksela, …, B. J. Mayer. 2008. A crucial role in cell spreading for the interaction of Abl PxxP motifs with Crk and Nck adaptors. *J. Cell Sci.* 121:3071–3082.

23. Shaul, Y. 2000. c-Abl: activation and nuclear targets. *Cell Death Differ.* 7:10–16.

24. Shishido, T., T. Akagi, …, H. Hanafusa. 2001. Crk family adaptor proteins trans-activate c-Abl kinase. *Genes Cells.* 6:431–440.

25. Sriram, G., C. Reichman, …, R. B. Birge. 2011. Phosphorylation of Crk on tyrosine 251 in the RT loop of the SH3C domain promotes Abl kinase transactivation. *Oncogene.* 30:4645–4655.

26. Savitski, M. M., F. B. Reinhard, …, G. Drewes. 2014. Tracking cancer drugs in living cells by thermal profiling of the proteome. *Science.* 346:1255784.

27. Palencia, A., E. S. Cobos, …, I. Luque. 2004. Thermodynamic dissection of the binding energetics of proline-rich peptides to the Abl-SH3 domain: implications for rational ligand design. *J. Mol. Biol.* 336:527–537.

28. Ferreon, J. C., and V. J. Hilser. 2004. Thermodynamics of binding to SH3 domains: the energetic impact of polyproline II (PII) helix formation. *Biochemistry.* 43:7787–7797.

29. Wang, C., N. H. Pawley, and L. K. Nicholson. 2001. The role of backbone motions in ligand binding to the c-Src SH3 domain. *J. Mol. Biol.* 313:873–887.

30. Ladbury, J. E., and S. T. Arold. 2011. Energetics of Src homology domain interactions in receptor tyrosine kinase-mediated signaling. *Methods Enzymol.* 488:147–183.

31. Zafra-Ruano, A., and I. Luque. 2012. Interfacial water molecules in SH3 interactions: getting the full picture on polyproline recognition by protein-protein interaction domains. *FEBS Lett.* 586:2619–2630.

32. Fersht, A. R. 1999. Structure and Mechanism in Protein Science. W.H. Freeman, New York.

33. Zhukov, A., and R. Karlsson. 2007. Statistical aspects of van 't Hoff analysis: a simulation study. *J. Mol. Recognit.* 20:379–385.

34. Otwinowski, Z., and W. Minor. 1997. Processing of x-ray crystallographic data in oscillation mode. *Methods Enzymol.* 276:307–326.

35. Adams, P. D., P. V. Afonine, …, P. H. Zwart. 2010. PHENIX: a comprehensive Python-based system for macromolecular structure solution. *Acta Crystallogr. D Biol. Crystallogr.* 66:213–221.

36. Emsley, P., and K. Cowtan. 2004. Coot: model-building tools for molecular graphics. *Acta Crystallogr. D Biol. Crystallogr.* 60:2126–2132.

37. Murshudov, G. N., P. Skubák, …, A. A. Vagin. 2011. REFMAC5 for the refinement of macromolecular crystal structures. *Acta Crystallogr. D Biol. Crystallogr.* 67:355–367.

38. Delaglio, F., S. Grzesiek, …, A. Bax. 1995. NMRPipe: a multidimensional spectral processing system based on UNIX pipes. *J. Biomol. NMR.* 6:277–293.

39. Keller, R. 2004. The Computer-Aided Resonance Assignment Tutorial. CANTINA, Reiskirchen, Germany.

40. Ikura, M., L. E. Kay, and A. Bax. 1990. A novel approach for sequential assignment of ^{1}H, ^{13}C, and ^{15}N spectra of proteins: heteronuclear triple-resonance three-dimensional NMR spectroscopy. Application to calmodulin. *Biochemistry.* 29:4659–4667.

41. Grzesiek, S., and A. Bax. 1992. An efficient experiment for sequential backbone assignment of medium-sized isotopically enriched proteins. *J. Magn. Reson.* 99:201–207.

42. Bax, A., and M. Ikura. 1991. An efficient 3D NMR technique for correlating the proton and ^{15}N backbone amide resonances with the α-carbon of the preceding residue in uniformly ^{15}N/^{13}C enriched proteins. *J. Biomol. NMR.* 1:99–104.

43. Kay, L. E., M. Ikura, …, A. Bax. 2011. Three-dimensional triple-resonance NMR spectroscopy of isotopically enriched proteins. 1990. *J. Magn. Reson.* 213:423–441.

44. Clubb, R. T., V. Thanabai, and G. Wagner. 1992. A constant-time three-dimensional triple-resonance pulse scheme to correlate intraresidue ^{1}HN, ^{15}N, and ^{13}C′ chemical shifts in ^{15}N–^{13}C labeled proteins. *J. Magn. Reson.* 97:213–217.

45. Wittekind, M., and L. Mueller. 1993. HNCACB, a high-sensitivity 3D NMR experiment to correlate amide-proton and nitrogen resonances with the α- and β-carbon resonances in proteins. *J. Magn. Reson. B.* B101:201–205.

46. Grzesiek, S., and A. Bax. 1993. Amino acid type determination in the sequential assignment procedure of uniformly ^{13}C/^{15}N-enriched proteins. *J. Biomol. NMR.* 3:185–204.

47. Bax, A., G. M. Clore, and A. M. Gronenborn. 1990. ^{1}H-^{1}H correlation via isotropic mixing of ^{13}C magnetization, a new three-dimensional approach for assigning ^{1}H and ^{13}C spectra of ^{13}C-enriched proteins. *J. Magn. Reson.* 88:425–431.

48. Wishart, D. S., C. G. Bigam, …, B. D. Sykes. 1995. ^{1}H, ^{13}C and ^{15}N chemical shift referencing in biomolecular NMR. *J. Biomol. NMR.* 6:135–140.

49. Ferrage, F., A. Reichel, …, R. Ghose. 2010. On the measurement of ^{15}N-^{1}H nuclear Overhauser effects. 2. Effects of the saturation scheme and water signal suppression. *J. Magn. Reson.* 207:294–303.

50. Lipari, G., and A. Szabo. 1982. Model-free approach to the interpretation of nuclear magnetic resonance relaxation in macromolecules. 1. Theory and range of validity. *J. Am. Chem. Soc.* 104:4546–4559.

51. Lipari, G., and A. Szabo. 1982. Model-free approach to the interpretation of nuclear magnetic resonance relaxation in macromolecules. 2. Analysis of experimental results. *J. Am. Chem. Soc.* 104:4559–4570.

52. Mandel, A. M., M. Akke, and A. G. Palmer, 3rd. 1995. Backbone dynamics of *Escherichia coli* ribonuclease HI: correlations with structure and function in an active enzyme. *J. Mol. Biol.* 246:144–163.

53. Cole, R., and J. P. Loria. 2003. FAST-Modelfree: a program for rapid automated analysis of solution NMR spin-relaxation data. *J. Biomol. NMR.* 26:203–213.

54. Fraternali, F., and L. Cavallo. 2002. Parameter optimized surfaces (POPS): analysis of key interactions and conformational changes in the ribosome. *Nucleic Acids Res.* 30:2950–2960.

55. Cavallo, L., J. Kleinjung, and F. Fraternali. 2003. POPS: a fast algorithm for solvent accessible surface areas at atomic and residue level. *Nucleic Acids Res.* 31:3364–3366.

56. Murphy, K. P., and E. Freire. 1992. Thermodynamics of structural stability and cooperative folding behavior in proteins. *Adv. Protein Chem.* 43:313–361.

57. Luque, I., and E. Freire. 2002. Structural parameterization of the binding enthalpy of small ligands. *Proteins.* 49:181–190.

58. Jankowski, W., T. Saleh, …, C. G. Kalodimos. 2012. Domain organization differences explain Bcr-Abl's preference for CrkL over CrkII. *Nat. Chem. Biol.* 8:590–596.

59. McCoy, A. J. 2007. Solving structures of protein complexes by molecular replacement with Phaser. *Acta Crystallogr. D Biol. Crystallogr.* 63:32–41.

60. Lim, W. A., F. M. Richards, and R. O. Fox. 1994. Structural determinants of peptide-binding orientation and of sequence specificity in SH3 domains. *Nature.* 372:375–379.

61. Xue, Y., T. Yuwen, …, N. R. Skrynnikov. 2014. Role of electrostatic interactions in binding of peptides and intrinsically disordered proteins to their folded targets. 1. NMR and MD characterization of the complex between the c-Crk N-SH3 domain and the peptide Sos. *Biochemistry.* 53:6473–6495.

62. Horn, J. R., D. Russell, …, K. P. Murphy. 2001. Van 't Hoff and calorimetric enthalpies from isothermal titration calorimetry: are there significant discrepancies? *Biochemistry.* 40:1774–1778.

63. Brown, A. M., and N. J. Zondlo. 2012. A propensity scale for type II polyproline helices (PPII): aromatic amino acids in proline-rich sequences strongly disfavor PPII due to proline-aromatic interactions. *Biochemistry.* 51:5041–5051.

64. Elam, W. A., T. P. Schrank, …, V. J. Hilser. 2013. Evolutionary conservation of the polyproline II conformation surrounding intrinsically disordered phosphorylation sites. *Protein Sci.* 22:405–417.

65. Tran, H. T., X. Wang, and R. V. Pappu. 2005. Reconciling observations of sequence-specific conformational propensities with the generic polymeric behavior of denatured proteins. *Biochemistry.* 44:11369–11380.

66. Ruzza, P., G. Siligardi, …, G. Borin. 2006. 4-Fluoroproline derivative peptides: effect on PPII conformation and SH3 affinity. *J. Pept. Sci.* 12:462–471.

67. McDonald, C. B., K. L. Seldeen, …, A. Farooq. 2009. SH3 domains of Grb2 adaptor bind to PXpsiPXR motifs within the Sos1 nucleotide exchange factor in a discriminate manner. *Biochemistry.* 48:4074–4085.

68. Rubini, C., P. Ruzza, …, A. Donella-Deana. 2010. Recognition of lysine-rich peptide ligands by murine contacting SH3 domain: CD, ITC, and NMR studies. *Biopolymers.* 94:298–306.

69. Ferreon, J. C., and V. J. Hilser. 2003. The effect of the polyproline II (PPII) conformation on the denatured state entropy. *Protein Sci.* 12:447–457.

70. Hamburger, J. B., J. C. Ferreon, …, V. J. Hilser. 2004. Thermodynamic mechanism and consequences of the polyproline II (PII) structural bias in the denatured states of proteins. *Biochemistry.* 43:9790–9799.

71. Breiten, B., M. R. Lockett, …, G. M. Whitesides. 2013. Water networks contribute to enthalpy/entropy compensation in protein-ligand binding. *J. Am. Chem. Soc.* 135:15579–15584.

72. Martin-Garcia, J. M., J. Ruiz-Sanz, and I. Luque. 2012. Interfacial water molecules in SH3 interactions: a revised paradigm for polyproline recognition. *Biochem. J.* 442:443–451.

73. Young, T., R. Abel, …, R. A. Friesner. 2007. Motifs for molecular recognition exploiting hydrophobic enclosure in protein-ligand binding. *Proc. Natl. Acad. Sci. USA.* 104:808–813.

74. Li, Z., and T. Lazaridis. 2006. Thermodynamics of buried water clusters at a protein-ligand binding interface. *J. Phys. Chem. B.* 110:1464–1475.

75. Palencia, A., A. Camara-Artigas, …, I. Luque. 2010. Role of interfacial water molecules in proline-rich ligand recognition by the Src homology 3 domain of Abl. *J. Biol. Chem.* 285:2823–2833.

76. Lu, Y., R. Wang, …, S. Wang. 2007. Analysis of ligand-bound water molecules in high-resolution crystal structures of protein-ligand complexes. *J. Chem. Inf. Model.* 47:668–675.

77. Ferreon, J. C., D. E. Volk, …, V. J. Hilser. 2003. Solution structure, dynamics, and thermodynamics of the native state ensemble of the Sem-5 C-terminal SH3 domain. *Biochemistry.* 42:5582–5591.

78. Manson, A., S. T. Whitten, …, V. J. Hilser. 2009. Characterizing the role of ensemble modulation in mutation-induced changes in binding affinity. *J. Am. Chem. Soc.* 131:6785–6793.

79. Akke, M., R. Bruschweiler, and A. G. Palmer. 1993. NMR order parameters and free energy: An analytical approach and its application to cooperative Ca^{2+} binding by calbinding D9k. *J. Am. Chem. Soc.* 115:9832–9833.

80. Yang, D., and L. E. Kay. 1996. Contributions to conformational entropy arising from bond vector fluctuations measured from NMR-derived order parameters: application to protein folding. *J. Mol. Biol.* 263:369–382.

81. Igumenova, T. I., A. L. Lee, and A. J. Wand. 2005. Backbone and side chain dynamics of mutant calmodulin-peptide complexes. *Biochemistry.* 44:12627–12639.

82. Ferreon, J. C., and V. J. Hilser. 2003. Ligand-induced changes in dynamics in the RT loop of the C-terminal SH3 domain of Sem-5 indicate cooperative conformational coupling. *Protein Sci.* 12:982–996.

83. Lee, A. L., and A. J. Wand. 2001. Microscopic origins of entropy, heat capacity and the glass transition in proteins. *Nature.* 411:501–504.

84. van Etten, R. A., P. Jackson, and D. Baltimore. 1989. The mouse type IV c-abl gene product is a nuclear protein, and activation of transforming ability is associated with cytoplasmic localization. *Cell.* 58:669–678.

85. Rubin, G. M., M. D. Yandell, …, S. Lewis. 2000. Comparative genomics of the eukaryotes. *Science.* 287:2204–2215.

86. Engh, R. A., and R. Huber. 1991. Accurate bond and angle parameters for x-ray protein structure refinement. *Acta Crystallogr. A.* 47:392–400.